Potential Vorticity Asymmetries and Tropical Cyclone Evolution in a Moist Three-Layer Model

LLOYD J. SHAPIRO

Meteorological Institute, University of Munich, Munich, Germany

(Manuscript received 28 January 1999, in final form 8 November 1999)

ABSTRACT

The role of potential vorticity (PV) asymmetries in the evolution of a tropical cyclone is investigated using a three-layer model that includes boundary layer friction, surface moisture fluxes, and a convergence-based convective parameterization. In a benchmark experiment, a symmetric vortex is first spun up on an f plane for 24 h. The symmetric vortex has a realistic structure, including a local PV maximum inside its radius of maximum wind (RMW). A weak azimuthal-wavenumber 2 PV asymmetry confined to the lower two layers of the model is then added to the vortex near the RMW. After an additional 2 h (for a total 26-h simulation), the asymmetric PV anomaly produces changes in the symmetric vortex that have significant differences from those in dry experiments with the present model or previous barotropic studies. A diagnosis of the contributions to changes in the symmetric wind tendency due to the asymmetry confirm the dominance of horizontal eddy fluxes at early times. The barotropic eddy kick provided by the anomaly lasts ~2 h, which is the damping timescale for the disturbance.

Additional experiments with an imposed isolated double-PV anomaly are made. Contrary to expectation from the dry experiments or barotropic studies, based on arguments involving ''wave activity,'' moving the anomaly closer to the center of the vortex or farther out does not change the overall evolution of the symmetric vortex. The physical mechanism responsible for the differences between the barotropic studies and those including moist physics as well as for the robustness of the response is established using a budget for the asymmetric vorticity. It is shown that the interactions between the asymmetries and the symmetric hurricane vortex at early times depend on realistic features of the model hurricane and not on interactions between the asymmetries and the boundary layer, which possibly depend on the convective parameterization. In particular, the changes in the symmetric wind tendency due to the asymmetry can be most simply explained by a combination of horizontal advection and damping of wave activity. In conjunction with horizontal advection and damping, the reversal of the radial vorticity gradient associated with the local PV maximum constrains the asymmetries to reduce the symmetric vorticity near the RMW. The location of the PV maximum controls the response to the extent that moving the PV anomaly radially inward or outward has no qualitative effect on the results. The longer-term evolution of the vortex is more problematic and may depend on the convective parameterization used.

1. Introduction

Second possibly only to track, the prediction of hurricane structure and intensity is the most important problem facing forecasters. Rapid intensification and the development of secondary eyewalls that lead to a cycle of intensification and weakening (Willoughby et al. 1982), are significant events in the evolution of a hurricane, whose origins are not well understood. Although a hurricane is essentially a symmetric system, it has become increasingly evident that asymmetric interactions between a hurricane and its environment play a critical role in the storm's development. Since the pioneering work of Pfeffer (1958; see also Pfeffer and Challa 1981), fluxes of angular momentum associated with asymmetries, especially in the upper troposphere, have been shown to play an important role (e.g., Molinari and Vollaro 1989) while more recent application of potential vorticity (PV) thinking has provided another perspective (Molinari et al. 1995).

Propagating and stationary spiral bands are ubiquitous asymmetric features of a hurricane (Willoughby et al. 1984), whose dynamics is central to understanding the storm's development. A recent study of Guinn and Schubert (1993) provides insight into the dynamics of spiral bands by demonstrating that those that develop in a shallow water primitive equation model can be understood as slowly evolving sheared PV disturbances associated with the advective (low frequency) component of the flow.

Most recently, Montgomery and Kallenbach (1997; hereafter MK97) and Möller and Montgomery (1999;

Corresponding author address: Dr. Lloyd J. Shapiro, Meteorological Institute, University of Munich, Theresienstr. 37, 80333 Munich, Germany.
E-mail: shapiro@meteo.physik.uni-muenchen.de

hereafter MM99) investigated the characteristics of spiral bands by studying the properties of outward-propagating vortex Rossby waves whose restoring mechanism is associated with the radial gradient of the storm vorticity. These waves provide a mechanism for transferring both energy from the hurricane's inner core to larger radii and disturbance vorticity up and down the basic state vorticity gradient. Thus, they are fundamental to the process by which a hurricane responds to a changing environment and may play an important role in hurricane intensification as well as in the creation of secondary eyewalls. The waves are mesoscale, with a radial scale ~10–25 km, consistent with outward-propagating bands observed in radar depictions of hurricanes. MM99 extended the quasilinear nondivergent analysis of MK97 to a weakly nonlinear asymmetric balance formulation, while Montgomery and Enagonio (1998; hereafter ME98) investigated tropical cyclogenesis in a three-dimensional nonlinear quasigeostrophic model.

MK97 used nondivergent and shallow water formulations to investigate the impact of asymmetries on barotropic vortices. In their simulations, monochromatic disturbances (with a given azimuthal wavenumber) were added to a barotropically stable symmetric vortex near its radius of maximum wind (RMW). The disturbances propagated energy radially, transferring energy to the basic state and eventually decaying (''symmetrizing'') due to the radial shear of the symmetric vortex. The symmetrizing disturbance accelerated the tangential wind near the radius at which the initial asymmetry was maximum, and decelerated it to a lesser degree at larger radii. ME98 used both monochromatic and azimuthally isolated initial conditions in a three-dimensional quasigeostrophic model, while MM99 used similar initial conditions in a nonlinear asymmetric balance shallow water model for large Rossby numbers, extending the results of MK97 to small but finite as well as large amplitude. In Figs. 6a and 12 of MM99, results from a shallow water version of the model used in the present study were shown. Quantitative agreement was found between the weakly nonlinear asymmetric balance formulation (Shapiro and Montgomery 1993) of MM99 and the primitive equation shallow water system for both weak and strong disturbances. In particular, after relatively short times, both formulations found a weak deceleration of the tangential wind near the vortex center [due to an ''induced'' inner-core asymmetry; see section 3b(1) of MM99] in addition to the acceleration and deceleration deduced by MK97.

The wave–mean–flow interaction predicted from the linear solutions in the simple models of MK97 led them to speculate on the role of convection in exciting the propagating Rossby wave disturbances. They noted, however, that ''further understanding of the impact of the small-scale PV bands requires an exploration of the eddy-forced circulation as well as their coupling to the boundary layer and convection.'' A hurricane is essentially a thermodynamic engine, and its eyewall and spiral band features are convective in nature. Therefore, any complete understanding of the role of asymmetric wave disturbances in a storm's evolution must include the influence of cumulus convection on both the symmetric vortex and the asymmetries. Guinn and Schubert (1993), MK97, and MM99 used barotropic models and could not incorporate the feedbacks associated with such processes; ME98 used a dry version of the quasigeostrophic model and parameterized moist processes via pulses in the PV field.

The studies of MK97, ME98, and MM99, as well as the more recent dry three-dimentional balance model results of Möller and Montgomery (2000) for strong vortices, have provided fundamental insights into interactions between asymmetries and a tropical cyclone. The symmetric vortices used by these authors, however, are unrealistic in several respects. In a real hurricane vortex, there is frictional convergence in the boundary layer and upward vertical motion in the eyewall region, which is strongest inside the RMW (see Fig. 19 of Jorgensen 1984). In close association with the updraft maximum, there is a local maximum in PV (also inside the RMW; see section 3b of Shapiro and Franklin 1995) due to its production in the convective eyewall. A thermally induced radial inflow feeds the eyewall updraft in the lower troposphere (Jorgensen 1984; Willouhby 1995; see also section 4 of Ooyama 1982). Neither the effect of the local PV maximum nor the lower-tropospheric inflow (and associated convergence) are included in the models of MK97, ME98, MM99, and Möller and Montgomery (2000).

Although hurricane models have used a wide variety of parameterization schemes, it is fair to say that in general, they all can reproduce the essential features of a realistic symmetric hurricane vortex, including those just noted. The simplest, fully interactive model that includes the essential elements of convection and its boundary layer roots is the classic three-layer model originally formulated in incompressible form by Ooyama (1969) and extended to a compressible fluid in isentropic coordinates by DeMaria and Pickle (1988). The model was used by these authors to simulate the symmetric evolution of a hurricane vortex and by Shapiro (1992) to isolate the mechanisms that determine the motion of a hurricane in an environment with vertical shear. The model includes boundary layer friction and surface moisture fluxes and uses a convective closure based on boundary layer convergence (mass flux) together with a budget for the moist static energy that determines the vertical mass redistribution. As seen in these papers and in the simulation in the present one (section 3), this parameterization scheme develops a realistic symmetric hurricane vortex. Alternate formulations to a convergence-based one are discussed in Smith (1997a). They include those that determine the convective mass flux from the assumption that in the presence of destabilization, due to surface sensible and latent heat fluxes, the boundary layer entropy stays in equilibrium

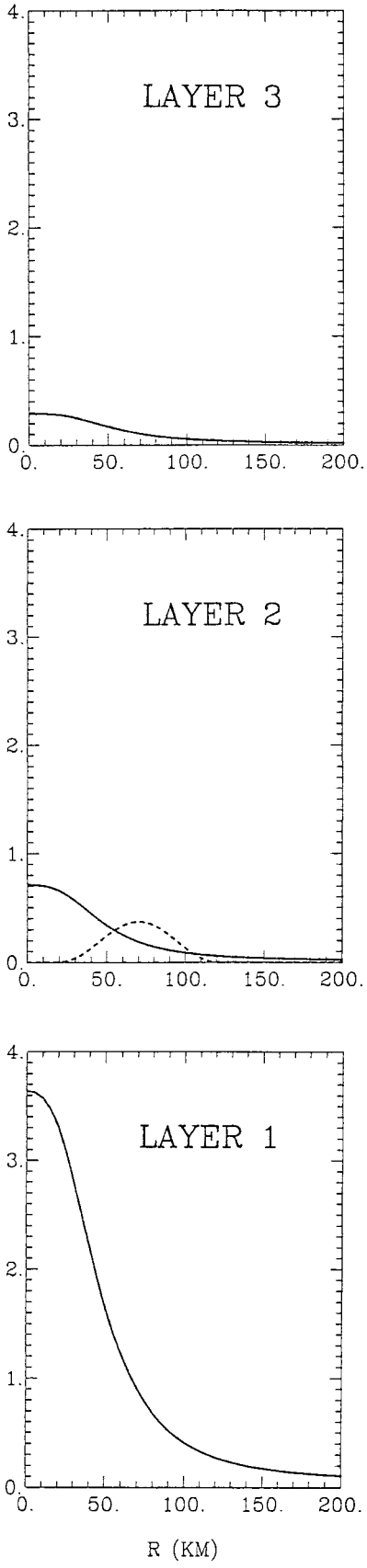

(Raymond 1995; Emanuel 1995). As shown very recently by J. Zehnder (J. Zehnder 1999, personal communication), a three-layer model using a version of Emanuel's (1995) scheme develops a realistic symmetric vortex as well.

The purpose of the present study is to elucidate the physical mechanisms underlying changes in hurricane structure and intensity. Specificially, a three-layer model will be used to determine the role of cumulus convection and the atmospheric boundary layer in the evolution of propagating vortex Rossby wave disturbances and their interactions with a developing hurricane. Some preliminary results from this study were presented in Shapiro (1998, 1999). The three-layer primitive equation model is the same one developed by Shapiro (1992), which utilizes the multinested model developed by Ooyama (described in DeMaria et al. 1992), which is based on the spectral application of a finite-element representation. In section 2, an experiment with a dry version of the three-layer model adds a weak azimuthal-wavenumber 2 PV asymmetry initially to a stable symmetric hurricanelike vortex near its RMW. The intensification of the symmetric vortex essentially replicates results of MK97 and MM99. The results are shown to be explained by relationships involving ''wave activity.''

When moist physics, including convection and boundary layer friction, is used, the results are more complex. The early evolution of the symmetric vortex (to $\sim$2 h) in the benchmark moist physics experiment, described in section 3, has significant differences from the dry simulations. A diagnosis of the contributions to changes in the symmetric wind tendency due to the asymmetry is made, confirming the dominance of horizontal eddy fluxes at early times. Additional experiments with an imposed isolated double-PV anomaly instead of wavenumber 2 are presented in section 4. When the double-PV anomaly is placed near the RMW, as in the benchmark moist physics experiment, the evolution of the symmetric vortex is, as expected, similar to that with the wavenumber 2 asymmetry. Contrary to expectations from the dry experiment or previous barotropic studies, however, moving the anomaly closer to the center of the vortex or further out does not change the overall evolution of the symmetric vortex. The physical mechanism responsible for the differences between the moist and dry simulations and robustness of the response is established using a budget for the asymmetric vorticity. It is shown that the interactions between the asymmetries and the symmetric hurricane vortex at early times depend on the realistic features of the model hurricane noted above and not on interactions between the

←

FIG. 1. Initial basic-state PV, $\overline{q}$ ($\times 10^{-6}$ s^{-1} m^{-1}), for dry experiment in layers 1, 2, and 3 are shown by solid lines. Initial amplitude of middle-layer (layer 2) azimuthal-wavenumber 2 PV asymmetry, $\hat{q}_2$ ($\times 10^{-7}$ s^{-1} m^{-1}), is shown by dashed line.

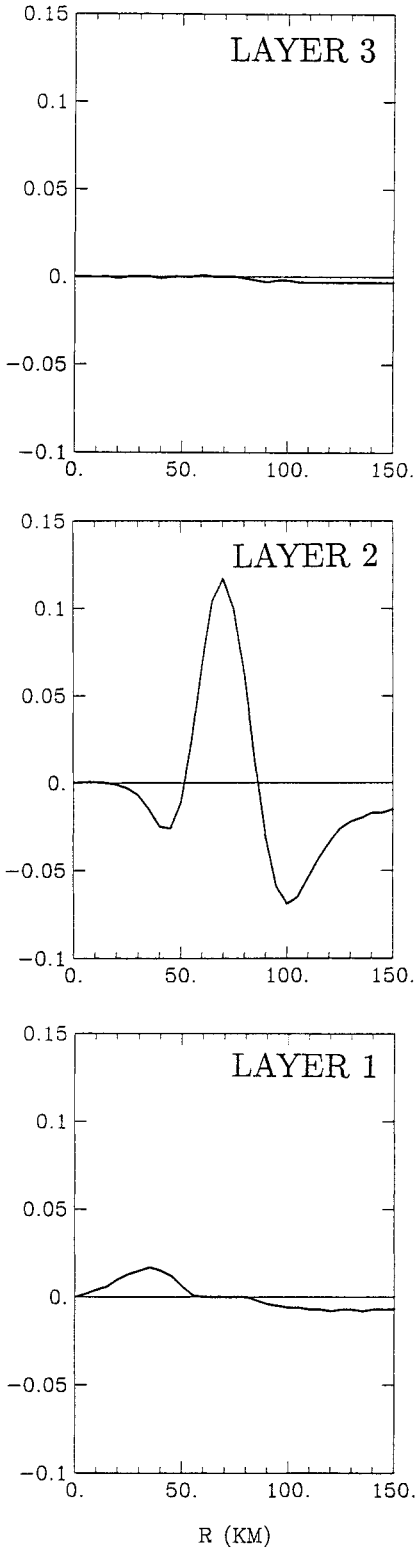

a)

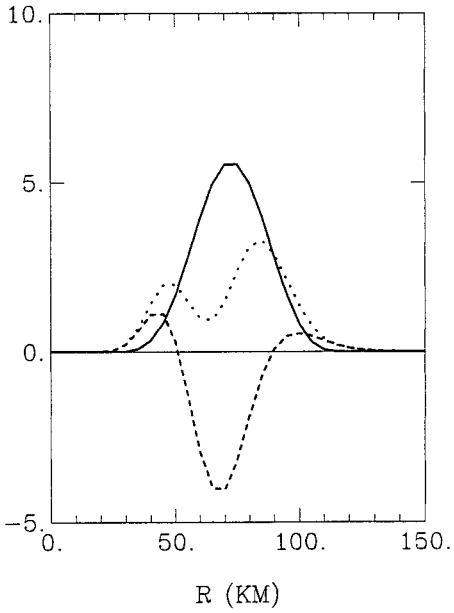

b)

asymmetries and the boundary layer, which possibly depend on the convective parameterization. As will be discussed in section 5, the long-term evolution of the vortex is more problematic and may depend on the convective parameterization used.

2. Dry experiment

Our dry simulation is made using the three-layer primitive equation isentropic coordinate model described in Shapiro (1992), omitting any boundary layer friction, horizontal diffusion, or convective parameterization. The model layer structure and thermodynamic parameters are the same as in Shapiro's (1992) and Demaria and Pickle's (1988) control simulation. A 7.5-km horizontal nodal spacing in the inner vortex core is required to resolve the propagating Rossby wave features and their interactions with each other and the mean vortex. The initial symmetric hurricane-like vortex in the lower and middle layers of the model is also used in section 3 of MK97, with a maximum tangential wind $\overline{V}_{1,2} = 36.8$ m s^{-1} at a radius $r = 75$ km (see MK97's Fig. 10); the vortex in the upper layer is $\overline{V}_3 = 0.75\overline{V}_1$. The PV of the vortex in each layer ($\overline{q}$; Fig. 1) decreases outward monotonically, indicating an exponentially stable basic state (Gent and McWilliams 1986; Montgomery and Shapiro 1995). As in Shapiro (1992), the PV is defined by

$$q = \eta/h,$$

where η is the absolute vorticity and h is the depth of the given layer. A weak azimuthal-wavenumber 2 PV asymmetry confined to the middle layer of the model is initially added to the symmetric vortex near its RMW. Wavenumber two is chosen, since it is the lowest azimuthal-wavenumber disturbance that does not have the complication of moving the vortex. The corresponding wind and height fields are deduced from the balance equation, linearized about the symmetric vortex so as to guarantee zero azimuthal mean of all asymmetric quantities. The magnitude of the initial PV anomaly in the middle layer ($\hat{q}_2$; Fig. 1) is 20% of $\overline{q}_2$ at the center of the anomaly. The associated (balanced) wind anomaly in the middle layer is $\sim$2 m s^{-1}, in the lower layer is $\sim$0.5 m s^{-1}, and in the upper layer is only $\sim$0.05 m s^{-1}. Figure 2a shows the changes in the tangential wind ($\Delta\overline{V}$) in each layer after 2 h, due to the asymmetric PV anomaly. The change (Δ) was evaluated by computing the difference between experiments made with and without the anomaly included.[1] As seen in Fig. 2a, in 2 h, the symmetrizing disturbance accelerates the middle-layer symmetric tangential wind near the radius at which the initial asymmetry is maximum and decelerates it to a lesser degree at larger and smaller radii. These changes are qualitatively the same as those deduced by MM99 and MK97. The magnitude of the acceleration is $\approx$the magnitude of the imposed wind anomaly. In the upper and lower layers, the symmetric vortex accelerates with correspondingly smaller magnitude.

As noted by MM99 and ME98, relationships involving wave activity can explain the changes in the symmetric barotropic vortex in their experiments as well as in those of MK97. In particular, in a nondivergent barotropic system, the budget for the asymmetric relative vorticity is

$$\frac{\partial\zeta'}{\partial t} + U'\frac{\partial\overline{\zeta}}{\partial r} + \frac{\overline{V}}{r}\frac{\partial\zeta'}{\partial\lambda} = 0, \tag{1}$$

where V is the tangential velocity, U is the radial velocity, and ζ is the vertical component of the relative vorticity; the overbar represents the azimuthal mean; and the prime deviates from the mean. This equation and the budget for the symmetric wind tendency

$$\frac{\partial\overline{V}}{\partial t} = -\overline{U'\zeta'} \tag{2}$$

can be used to derive the tendency of the symmetric wind in terms of changes in $\overline{\zeta'^2}$, the so-called wave activity for this system:

$$\frac{\partial\overline{V}}{\partial t} = \left[\frac{1}{2}\frac{\partial(\overline{\zeta'^2})}{\partial t}\right]\Big/\frac{\partial\overline{\zeta}}{\partial r}. \tag{3}$$

A similar derivation was made in a barotropic nondivergent context for wave disturbances in a zonal shear flow by Held and Hoskins (1985) [cf. their Eq. (3.7)], including the effect of linear diffusion. The sign of the contributions to (3) are such that a symmetrically stable vortex (with a monotonically decreasing vorticity, $\partial\overline{\zeta}/\partial r < 0$) will tend to decelerate ($\partial\overline{V}/\partial t < 0$) due to a locally growing disturbance [increasing wave activity; $\partial(\overline{\zeta'^2})/\partial t > 0$] and will tend to accelerate due to a locally decaying one. These relationships explain the patterns of acceleration and deceleration seen in Fig. 2a. Figure 2b shows the initial wave activity in the middle layer, its value

[1] A symmetric vortex on an f plane does not evolve. In the present model, numerical approximations lead to a very slow vortex drift, which is removed in this method of evaluating the change due to the anomaly.

←

FIG. 2. (a) Change in basic-state tangential wind, $\Delta\overline{V}$ (m s^{-1}); in layers 1, 2, and 3 for dry experiment after 2 h. (b) Middle-layer wave activity $\overline{\zeta_2'^2}$ ($\times 10^{-9}$ s^{-2}) initially (solid line), after 2 h (dotted line), and their difference (dashed line) for dry experiment.

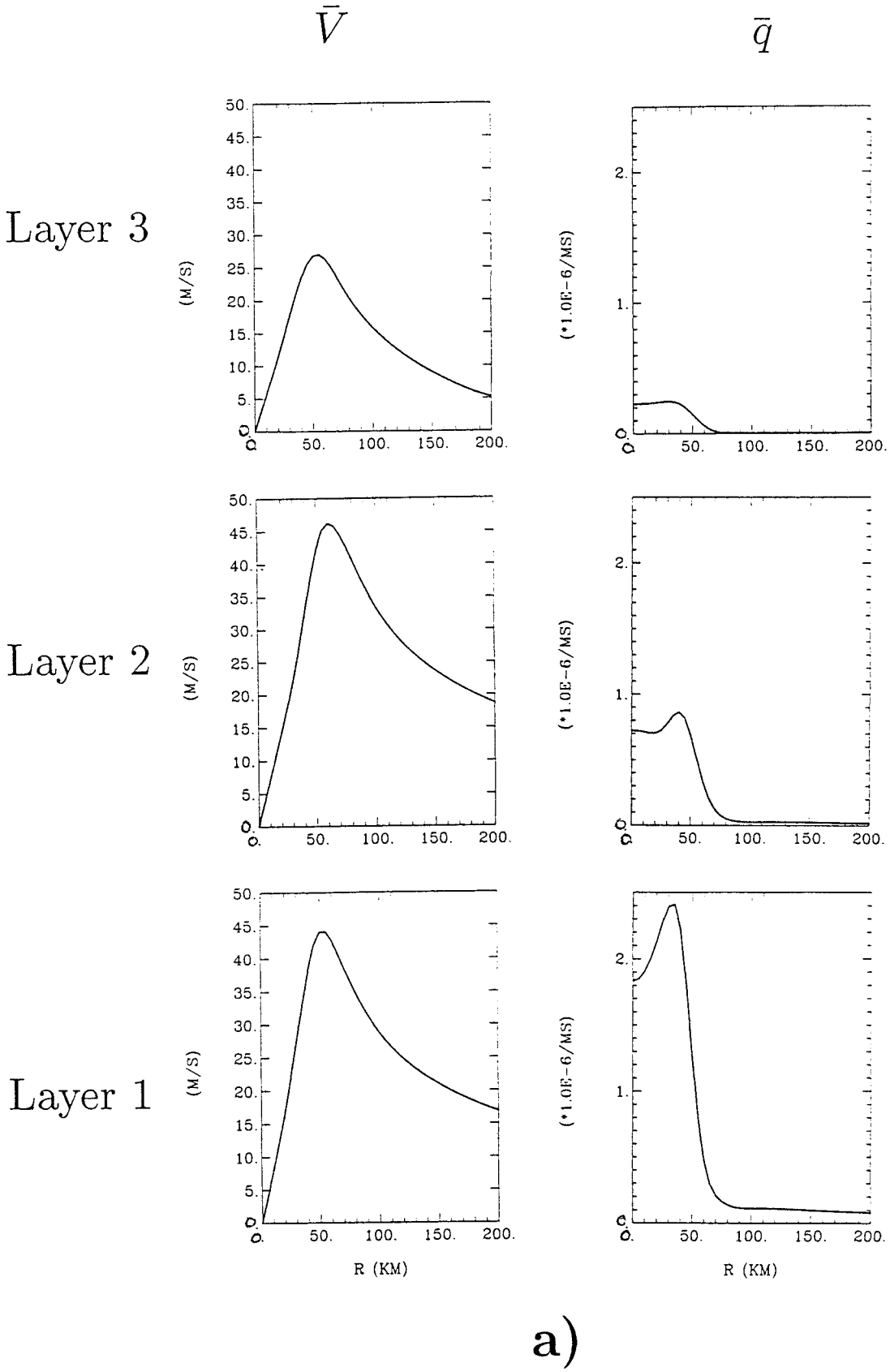

a)

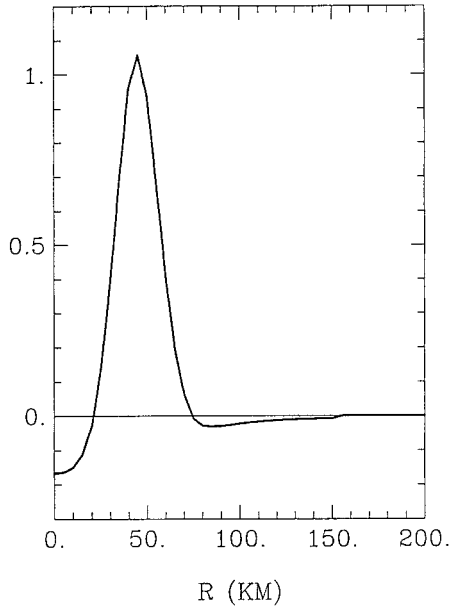

FIG. 3 (*Continued*)

after 2 h, and its change for the present experiment. An acceleration is seen where the wave activity decreases in the region of the initial anomaly, and a deceleration is seen both farther from the center (where the wave activity increases due to radial propagation) as well as closer to the center (due to the inward induced anomaly). The generalization of (2) and (3) to a divergent system with diffusion is made in the following sections, where implications for the evolution of a vortex with a nonmonotonic vorticity distribution are considered.

3. Early evolution: Benchmark moist experiment

As noted in the introduction, a realistic hurricane vortex has features, including a local PV maximum inside the RMW, that are not present in the dry simulation of section 2 or in the studies of MK97, MM99, and ME98. These features may have a significant impact on the interaction between PV asymmetries and the vortex. Interactions between the asymmetries and the boundary layer and convection may also alter the evolution of the asymmetries and the symmetric vortex. Thus, in principle, the evolution of the vortex with moist physics included could be very different from that found in section 2. In this section, results will be shown from an experiment with the moist version of the three-layer model, described in Shapiro (1992). In this model, the magnitude of the convective mass flux is proportional to the boundary layer convergence. Changes in the boundary layer depth have an impact on the convection, and thus, the evolution of the model vortex. For simplicity as well as to avoid ambiguities of interpretation when an anomaly is added to a vortex, the present model experiments are made with the depth of the boundary layer taken to be constant rather than a variable boundary layer depth, as in Shapiro (1992) and section 2. Consistency with the model's thermodynamic structure requires the potential temperature of the middle (entrainment) layer of the model to be taken equal to that of the lower (boundary) layer.[2] The model uses a second-order horizontal diffusion with a divergence-dependent coefficient, as formulated by Ooyama (1984). Discussion of the diffusion is given in section 2 of Shapiro (1992). As in that paper, the magnitude of the diffusion coefficient is chosen to be as small as possible while still controlling the production of energy near the shortest representable wavelength. All other physical parameters are the same as in Shapiro (1992).

In the benchmark experiment, a symmetric vortex is first spun up on an f plane for 24 h in order to develop a realistic hurricanelike structure. At this time, the maximum middle-layer tangential wind is 46 m s^{-1} at $r \sim 60$ km, and there is a local PV maximum and a reversal in the radial PV gradient inside the RMW in all three layers (Fig. 3a). The local maximum is due to PV production by convection in the model eyewall. The vertical velocity at the top of the boundary layer ($\overline{w}_{BL}$; Fig. 3b), which is proportional to the convective mass flux, is maximum near a 45-km radius inside the RMW. As in the dry case, an azimuthal-wavenumber 2 PV asymmetry confined to the middle (entrainment) layer of the model is then added to the vortex near its RMW, with corresponding wind and height fields deduced from the linearized balance equation.[3] The initial PV asymmetry (Fig. 4) is confined to radii between 20 and 80 km, with maximum amplitude equal to 20% of the symmetric PV at $r = 50$ km. The wind field in balance with the initial

[2] If the boundary layer depth is constant, then the linear system to be solved for layer depth anomalies in terms of geopotential anomalies [DeMaria and Pickle's Eq. (2.33)] is overdetermined unless the geopotential anomalies and potential temperatures of the lowest two layers are equal.

[3] Since the potential temperatures of the middle and lower (boundary) layers are equal, the geopotential anomalies in these two layers are also equal [see footnote 2 and DeMaria and Pickle's Eq. (2.33)]. The wind anomalies in balance with the geopotentials in these two layers are equal as well, as are the vorticity anomalies. The combination of vorticity anomaly and the constraint of constant boundary layer depth mandates that the balanced fields have a nonzero PV anomaly in the lower layer.

←

FIG. 3. Symmetric vortex for benchmark moist experiment spun up to 24 h; (a) tangential wind, $\overline{V}$ (m s^{-1}), and potential vorticity, $\overline{q}$ ($\times 10^{-6}$ s^{-1} m^{-1}), for layers 1, 2, and 3; (b) vertical velocity at the top of the boundary layer, $\overline{w}_{BL}$ (m s^{-1}).

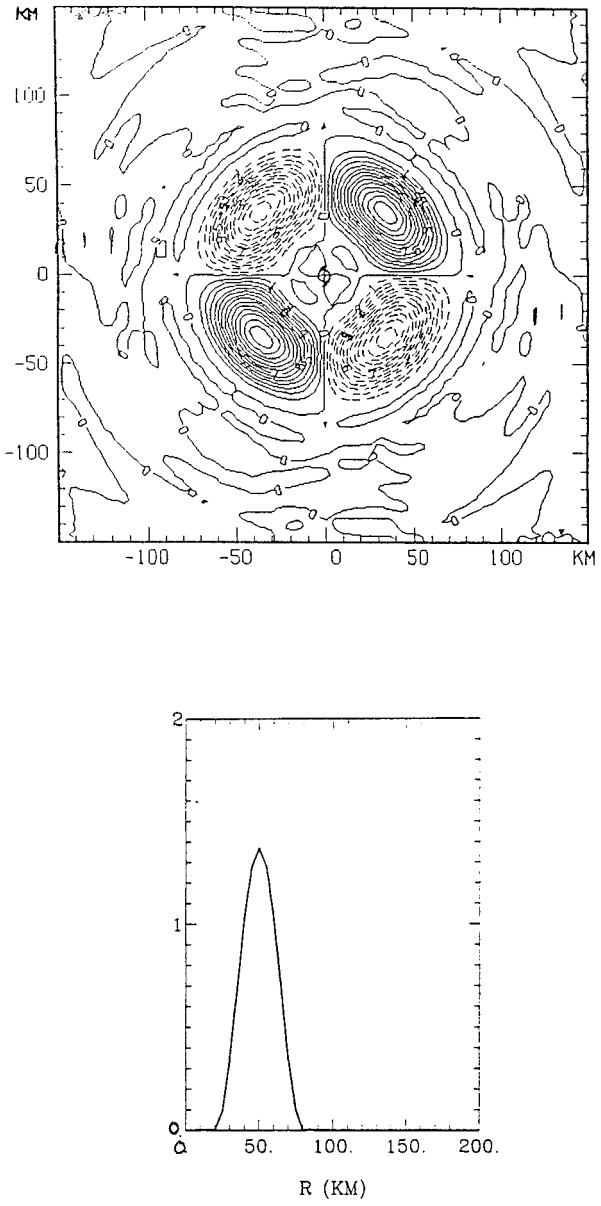

FIG. 4. Middle-layer azimuthal-wavenumber 2 PV anomaly added to spunup (time = 24 h) symmetric vortex in benchmark experiment. Top panel is horizontal distribution of PV ($\times 10^{-8}$ s^{-1} m^{-1}); bottom panel is amplitude, $\hat{q}_2$ ($\times 10^{-7}$ s^{-1} m^{-1}).

asymmetry has an amplitude ~3 m s^{-1} in both the middle and bottom (frictional boundary) layers.

Figure 5 shows the changes in the tangential wind in each layer and vertical velocity at the top of the boundary layer ($\Delta\overline{w}_{BL}$) due to the asymmetric PV anomaly. In order to isolate the effect of the asymmetries on the evolution of the vortex, the change is evaluated by computing the difference between experiments made with and without the anomaly included, as in the dry experiment in section 2. After 30 min (for a total 24-h, 30-min simulation), the middle-layer tangential wind accelerated by $\Delta\overline{V}_2 = 0.17$ m s^{-1} inside $r \sim 45$ km and decelerated by $\Delta\overline{V}_2 = -0.09$ m s^{-1} outside (Fig. 5a). The boundary layer tangential wind change, $\Delta\overline{V}_1$, is shifted radially inward from the middle layer and has a weaker acceleration. The change in the upper-layer tangential wind, $\Delta\overline{V}_3$, is much stronger and qualitatively different than the corresponding changes in the dry experiment in section 2 due to convective mass and momentum transports into the upper layer in the present moist experiment. The acceleration of the middle-layer tangential wind increases after 1 h (time = 25 h; Fig. 5b) to 0.28 m s^{-1}; there is a net intensification of the vortex due to the asymmetry, with the change in the central surface pressure $\Delta p_s = -0.06$ mb. After 2 h (time = 26 h; Fig. 5c), the acceleration and net intensification of the vortex decrease. Although the pattern of acceleration and deceleration in the middle-layer tangential wind appears qualitatively similar to the dry results of section 2 (see Fig. 2a), there are significant differences. The maximum acceleration ($\Delta\overline{V}_2 > 0$) is at $r \sim 35$ km, well inside the center of the initial imposed PV anomaly, which is at $r = 50$ km. This result is unlike the dry simulation of section 2 or MK97 and MM99, where the maximum acceleration was near the center of the initial anomaly. In the present simulation, the acceleration at $r = 50$ km is, in fact, close to zero. Farther out, there is a deceleration, which is maximized at $r \sim 60$ km, near the RMW. These changes correspond to an inward movement of the tangential wind profile together with a weakening of the maximum wind. In the following section, the physical mechanism responsible for the differences between the moist and dry results will be established. The changes in the tangential wind and the associated changes in vorticity induce corresponding changes in the vertical velocity at the top of the boundary layer, $\Delta\overline{w}_{BL}$ (bottom panels of Fig. 5), with a maximum increase at $r \sim 25$ km and a maximum decrease at $r \sim 45$ km, the radius of maximum $\overline{w}_{BL}$ (Fig. 3b).

A diagnosis of the contributions to changes in the symmetric wind tendency due to the asymmetry confirm the dominance of horizontal eddy fluxes in the early evolution of the vortex. Neglecting the small contribution from vertical diffusion, the tendency of the middle-layer symmetric wind is given by

$$\frac{\partial \overline{V}}{\partial t} = -\overline{U'\zeta'} - \overline{U}\,\overline{\eta} + \nabla \cdot [\overline{\nu}\nabla\overline{V}] + \epsilon, \qquad (4)$$

where ν is the horizontal diffusion; the subscript "2," representing the middle layer, has been omitted from all quantities for notational simplicity. This equation is the generalization of (2) to a divergent system with diffusion. The first term on the right-hand side of the equation is the eddy radial vorticity flux, the second is the symmetric radial vorticity flux, the third is the contribution from symmetric horizontal diffusion, and ϵ is the small

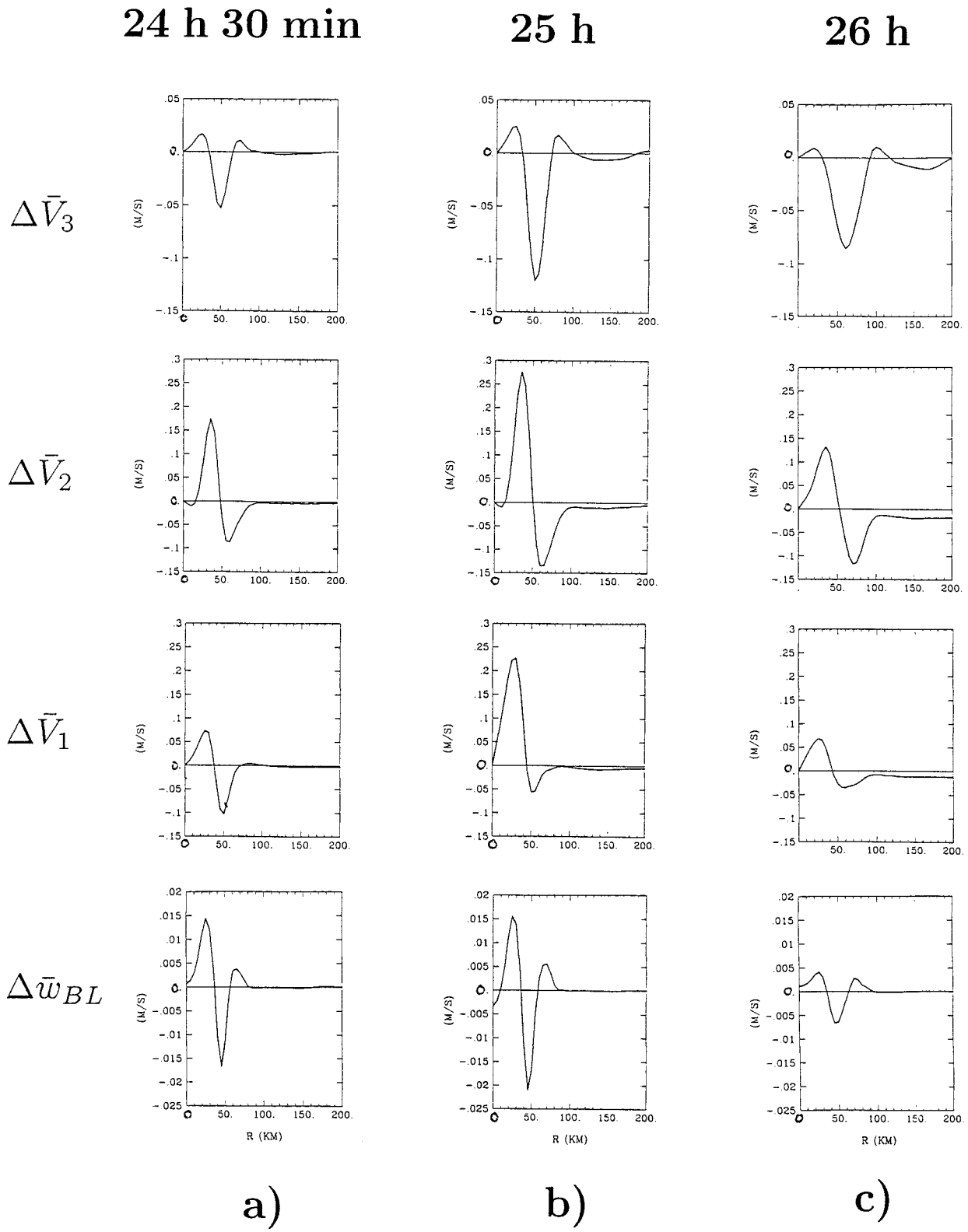

FIG. 5. Change in basic-state tangential wind, $\Delta\overline{V}$ (m s^{-1}); in layers 1, 2, and 3; and vertical velocity at top of boundary layer, $\Delta\overline{w}_{BL}$ (m s^{-1}), due to asymmetry in benchmark experiment after (a) 30 min (time = 24 h 30 min), (b) 1 h (time = 25 h), (c) 2 h (time = 26 h).

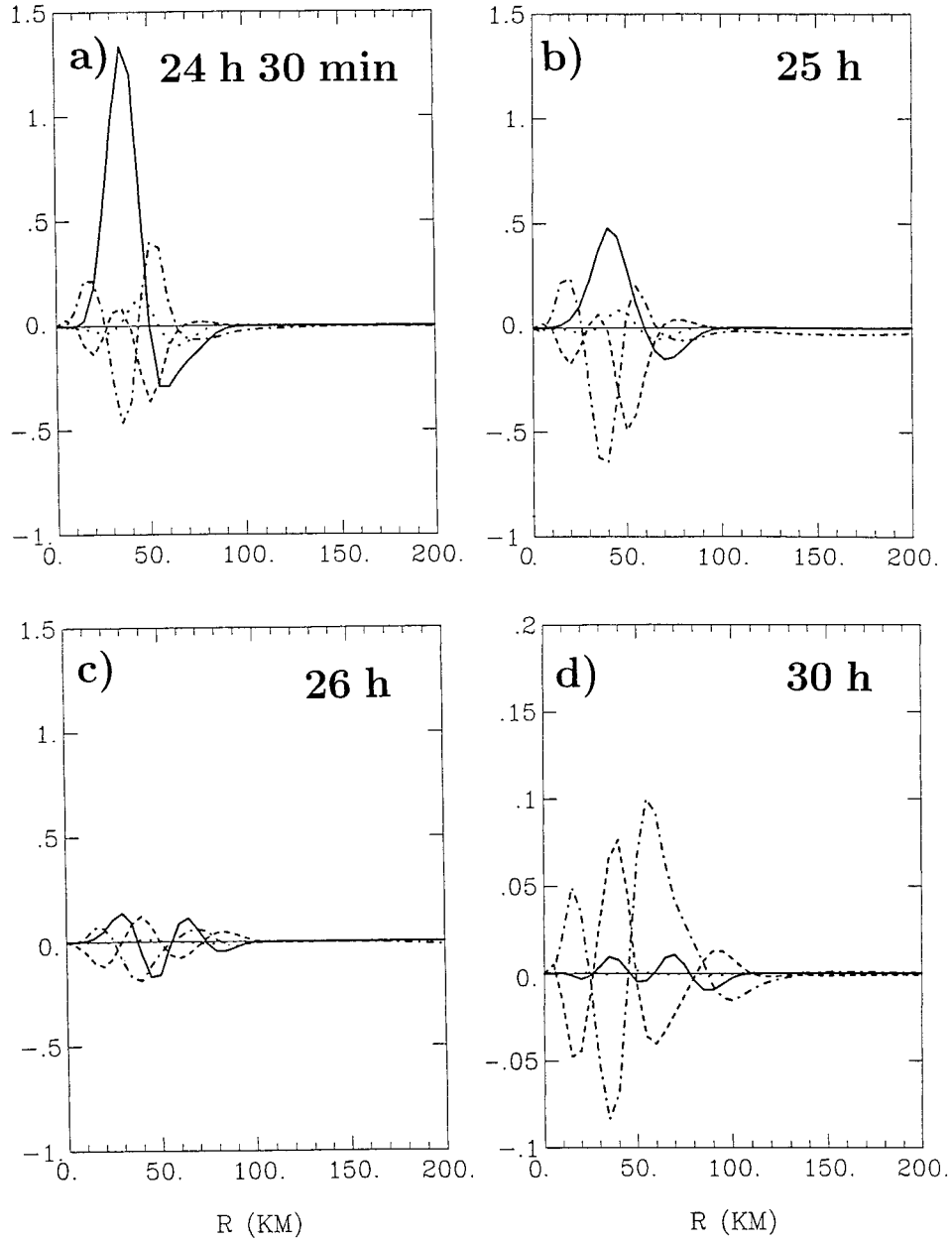

FIG. 6. Contributions to change in middle-layer symmetric wind tendency due to the asymmetry, $\Delta\partial\overline{V}_2/\partial t$ (m s^{-1} in 2 h), from horizontal eddy vorticity flux (solid line); change in symmetric vorticity flux (dashed line); change in symmetric horizontal diffusion (dash-dotted line); and eddy horizontal diffusion (dotted line) after (a) 30 min (time = 24 h 30 min), (b) 1 h (time = 25 h), (c) 2 h (time = 26 h), (d) 6 h (time = 30 h). Note different vertical scale in (d).

contribution from eddy horizontal diffusion.[4] The change in the symmetric wind tendency due to the asymmetry is then

$$\Delta\frac{\partial\overline{V}}{\partial t} = -\overline{U'\zeta'} + \Delta[-\overline{U}\,\overline{\eta}] + \Delta[\boldsymbol{\nabla}\cdot(\overline{\nu}\boldsymbol{\nabla}\overline{V})] + \epsilon. \quad (5)$$

At 24 h 30 min (Fig. 6a), the contribution of the eddy vorticity flux term is much greater than the other terms. The eddy kick provided by the imposed asymmetry lasts ~2 h. By 26 h (Fig. 6c), the contribution from the eddy flux decreases to about a tenth of its value at 24 h, 30 min. During this same period, the changes in the sym-

[4] In a region of boundary layer convergence in a convectively stable sounding, (4) would also include a source due to vertical advection. No such region of stable convergence occurs in any of the diagnostics presented.

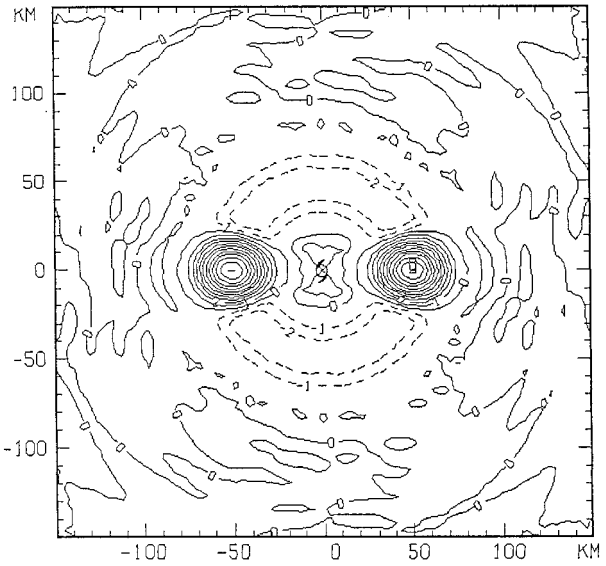

FIG. 7. Middle-layer PV anomaly ($\times 10^{-8}$ s^{-1} m^{-1}) added to spunup (time = 24 h) symmetric vortex in double-cluster experiment centered at $r = 50$ km.

metric vorticity flux and symmetric horizontal diffusion oppose the eddy flux (most strongly near 25 h; see Fig. 6b) but do not change its qualitative effect. The dependence of the vortex evolution on the location of the imposed asymmetry is investigated in the following section.

4. Early evolution: Double-cluster experiments

While MK97 analyzed the potential effect of monochromatic initial asymmetries on the intensification of a barotropic vortex, MM99 and ME98 studied the effect of azimuthally isolated anomalies as well. Additional experiments with an imposed isolated double-PV anomaly instead of wavenumber 2 have been completed with the moist version of the present model. As in the benchmark experiment, the PV anomaly is added to the middle layer of the model after the initial 24-h spinup. In the first double-cluster experiment, just as in the benchmark experiment, the PV anomaly (Fig. 7) is centered at $r = 50$ km, is confined between $r = 20$ and 80 km (see bottom panel of Fig. 4), and has maximum amplitude equal to 20% of the symmetric PV at $r = 50$ km. The azimuthal average is removed from the PV anomaly so as not to change the structure of the symmetric vortex. As expected, the evolution of the vortex after the anomaly is added is very similar to that in the benchmark experiment. In particular, after 30 min, the tangential wind accelerates inside $r \sim 45$ km and decelerates outside (Fig. 8b); these changes lead to a net intensification of the vortex. As in the benchmark experiment, the maximum acceleration of the vortex is at $r \sim 35$ km and deceleration is at $r \sim 60$ km. At this time, horizontal eddy vorticity fluxes (not shown) dominate the change in the symmetric wind tendency.

From the wave activity analysis of the dry results in section 2, a change in the radial location of the asymmetry would be expected to modify the evolution of the vortex. In particular, if the anomaly is displaced radially outward, then the induced acceleration of the symmetric vortex would be expected to be displaced outward as well. Experiments have been made with the center of the asymmetry moved from $r = 50$ km inward to 30 km and outward to 70 and 90 km. Contrary to expectation, these changes do not modify the overall evolution of the symmetric vortex. As shown in the four panels of Fig. 8, although the center of the imposed anomaly ranges over a radial distance of 60 km, the structure of $\Delta\overline{V}_2$ changes very little. In *every* case, after 30 min, there is a maximum acceleration at $r \sim 35$ km and a maximum deceleration at $r \sim 60$ km.

The physical mechanism responsible for the robustness of this result can be diagnosed using a budget for the asymmetric vorticity. Neglecting small contributions from vertical diffusion [as in (4)], the linearized vorticity budget for the middle-layer asymmetric vorticity is

$$\frac{\partial \zeta'}{\partial t} + \overline{U}\frac{\partial \zeta'}{\partial r} + U'\frac{\partial \overline{\zeta}}{\partial r} + \frac{\overline{V}}{r}\frac{\partial \zeta'}{\partial \lambda} + \overline{\eta}\delta' + \zeta'\overline{\delta} - \overline{\nu}\nabla^2\zeta' + \mathcal{D}' = 0, \tag{6}$$

where δ is the divergence and $\mathcal{D}'$ represents additional terms involving horizontal diffusion, ν; as in (4) and (5), the subscript ''2'' has been omitted from all quantities. This equation is the generalization of (1) to a divergent system with diffusion. Multiplication by ζ' and averaging azimuthally gives an equation for the evolution of wave activity, $\overline{\zeta'^2}$,

$$\frac{1}{2}\frac{\partial(\overline{\zeta'^2})}{\partial t} + \frac{1}{2}\overline{U}\frac{\partial(\overline{\zeta'^2})}{\partial r} + \overline{U'\zeta'}\frac{\partial \overline{\zeta}}{\partial r} + \overline{\eta}\,\overline{\delta'\zeta'} + \overline{\delta}\,\overline{\zeta'^2} - \overline{\nu}\,\overline{\zeta'\nabla^2\zeta'} + \overline{\zeta'\mathcal{D}'} = 0. \tag{7}$$

At early times, when horizontal eddy fluxes dominate the change in the symmetric wind tendency due to the asymmetry, (5) reduces to the simple budget

$$\Delta\frac{\partial \overline{V}}{\partial t} \approx -\overline{U'\zeta'}.$$

Substitution from (7) then gives for early times,

$$\Delta\frac{\partial \overline{V}}{\partial t} \approx \left[1 \Big/ \frac{\partial \overline{\zeta}}{\partial r}\right]\left[\frac{1}{2}\frac{\partial(\overline{\zeta'^2})}{\partial t} + \frac{1}{2}\overline{U}\frac{\partial(\overline{\zeta'^2})}{\partial r} + \overline{\eta}\,\overline{\delta'\zeta'} + \overline{\delta}\,\overline{\zeta'^2} - \overline{\nu}\,\overline{\zeta'\nabla^2\zeta'} + \overline{\zeta'\mathcal{D}'}\right]. \tag{8}$$

This equation, which is the generalization of (3), allows one to diagnose the contributions to the symmetric wind

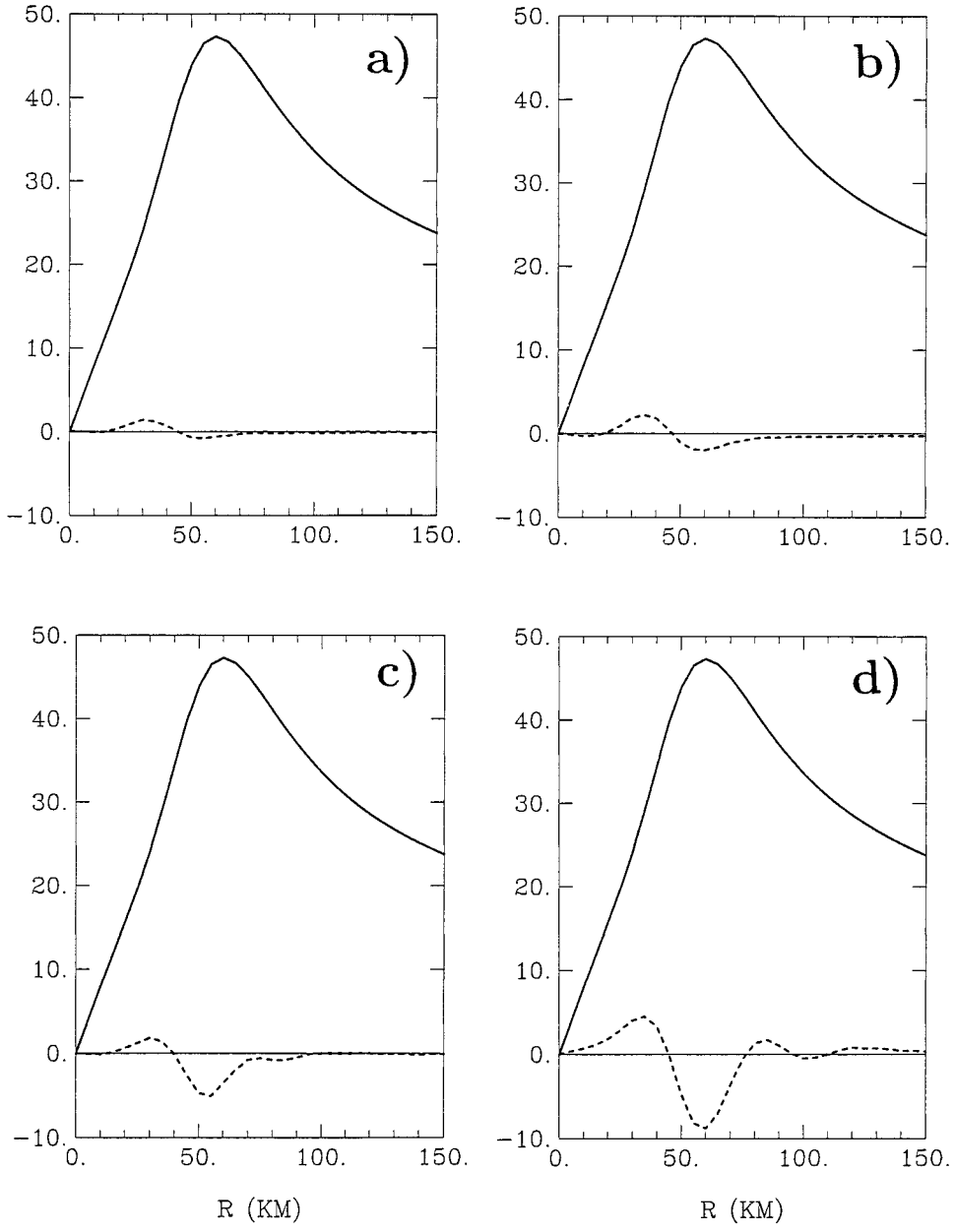

FIG. 8. Initial middle-layer symmetric tangential wind, $\overline{V}_2$ (m s^{-1}, solid line), and change ($\times 10^{-2}$ m s^{-1}, dashed line), after 30 min (time = 24 h, 30 min) in double-cluster experiment centered at r = (a) 30 km, (b) 50 km, (c) 70 km, (d) 90 km.

tendency from the total advective (Lagrangian) time change [first two terms on the right-hand side of (8)], vortex stretching (the second two terms), and diffusive damping (the last two terms).

In the present study, there is a local maximum in $\overline{\zeta}_2$ (Fig. 9) and a corresponding change in the sign of $\partial\overline{\zeta}_2/\partial r$, at $r \sim 40$ km, due to PV production by convection (see discussion of Fig. 3a in section 2). Near this radius, (8) becomes ill-posed so that the alternative form in terms of the vorticity budget,

$$\frac{\partial\overline{\zeta}}{\partial r}\Delta\frac{\partial\overline{V}}{\partial t} \approx -\overline{U'\zeta'}\frac{\partial\overline{\zeta}}{\partial r} = \frac{1}{2}\frac{\partial(\overline{\zeta'^2})}{\partial t} + \frac{1}{2}\overline{U}\frac{\partial(\overline{\zeta'^2})}{\partial r} + \overline{\eta}\,\overline{\delta'\zeta'} + \overline{\delta}\,\overline{\zeta'^2} - \overline{\nu}\,\overline{\zeta'\nabla^2\zeta'} + \overline{\zeta'\mathcal{D}'}, \quad (9)$$

will be used here. The horizontal eddy vorticity flux in the middle layer [right-hand side of the first line of (9)], the total advective time change [first two terms on the

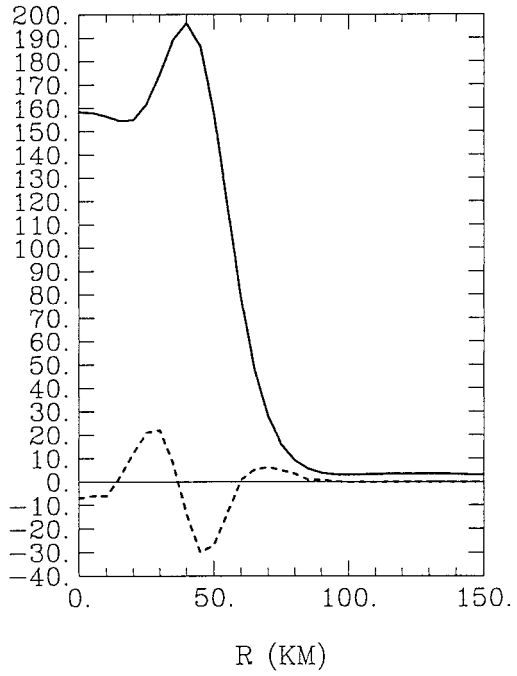

FIG. 9. Middle-layer symmetric vorticity, $\overline{\zeta}_2$ ($\times 10^{-5}$ s^{-1}, solid line), and change, $\Delta\overline{\zeta}_2$ ($\times 10^{-7}$ s^{-1}, dashed line), after 30 min (time = 24 h, 30 min) in double-cluster experiment centered at $r = 50$ km.

second line of (9)], and their difference, are shown after 30 min in Fig. 10 for all of the double-blob experiments.

The initial and final middle-layer wave activity as well as its change after 30 min for the initial anomaly centered at $r = 90$ km, as an example, are shown in Fig. 11. The initial distribution and change in the tangential wind for this case were shown in Fig. 8d. While the magnitude of the initial anomaly decays, a second maximum is induced near $r = 60$ km [for a discussion of the induced anomaly, see section 3b(1) of MM99]. As seen in Fig. 10d, for this experiment, the total advective time change terms in (9) explain the horizontal eddy fluxes (and thus the change in $\overline{V}$) very well inside $r \sim 75$ km, in the region of the induced anomaly. As shown in Fig. 12a, for the same experiment, the local tendency of wave activity alone gives poorer agreement in this region; $\overline{\nu}$ contributes to the balance. Outside $r \sim 75$ km, where the initial anomaly decays, the difference between the eddy horizontal vorticity flux term and the total advective time change (Fig. 10d) is positive, requiring a positive contribution to balance the negative advection. The decay of the vorticity can be explained by effective damping from horizontal diffusion [the last two terms in (9)]. Based on the ratio between the residual difference in Fig. 10d ($\sim 0.1 \times 10^{-11}$ s^{-3}) and the amplitude of the wave activity after 30 min in Fig. 11 ($\sim 7 \times 10^{-9}$ s^{-2}), the effective damping rate is $\overline{D} \sim 1.4 \times 10^{-4}$ s^{-1}. The damping timescale, $1/\overline{D} \sim$ 2 h, is consistent with the decay time for the eddy vorticity fluxes found in both the benchmark and the double-blob experiments. As seen in Fig. 12b, inclusion of the divergence terms in (9) requires a balance with an additional positive contribution from diffusion in the region of the induced anomaly.

For each of the four cases presented in Fig. 10 (a, b, c, and d), the horizontal eddy vorticity fluxes can be most simply explained by a combination of horizontal advection and damping of the initial anomaly. Advection gives a positive contribution to the vorticity budget (9) away from the initial anomaly, and damping and advection tend to balance in the region of the anomaly. The net effect is to have $-\overline{U'\zeta'}(\partial\overline{\zeta}/\partial r) \approx (\partial\overline{\zeta}/\partial r)\Delta(\partial\overline{V}/\partial t) > 0$ in every case (Figs. 10a,b,c,d) at $r \sim 35$ and 55 km. Since $(\partial\overline{\zeta}/\partial r)\Delta(\partial\overline{V}/\partial t) > 0$, the sign of $\Delta(\partial\overline{V}/\partial t)$ there is the same as the sign of $\partial\overline{\zeta}/\partial r$. For the symmetric vortex in these experiments, $\partial\overline{\zeta}_2/\partial r$ changes sign at $r \sim 40$ km; it is positive inside this radius (to ~20 km) and negative outside (Fig. 9). Consistent with the previous discussion, $\Delta(\partial\overline{V}_2/\partial t) > 0$ at $r \sim 35$ km and <0 at $r \sim 55$ km, as in Figs. 5a and 8. The change in middle-layer vorticity is therefore negative ($\Delta\overline{\zeta}_2 < 0$) between these radii (as in Fig. 9 for the initial anomaly centered at $r = 50$ km). This change has an impact on the longer-term evolution of the vortex, discussed in the following section.

The terms on the second line of (9) represent the contributions of the middle-layer asymmetry to the evolution of the middle-layer symmetric wind. Horizontal advection (the first two terms) and horizontal diffusion (the last two terms) are local to the middle layer. Only those terms involving vortex stretching (the second two terms) relate to interactions between the middle and boundary layer via convectively forced convergence. The fourth term involves middle-layer mean convergence, $-\overline{\delta}_2$, which is driven primarily by entrainment into the eyewall updraft. As noted in section 1, this is a realistic feature of the symmetric hurricane. The third term involves asymmetric convergence, $-\delta'_2$, which in the present convergence-based convective parameterization, is approximately in phase with the asymmetric vorticity, ζ'_2, due to an Ekman-like convergence in the boundary layer. Analysis indicates, however, that for the early times considered in this section, the third term is much smaller than the fourth term. The divergence terms, such as those evaluated in Fig. 12b, are completely dominated by the term involving the product of mean convergence and wave activity. Thus, the difference between the present moist results and those of the dry experiment in section 2 are due to realistic features of the symmetric vortex in the moist experiments and the resulting interactions with the vorticity asymmetry and *not* to coupling of the asymmetry with the boundary layer, which could depend on the convective parameterization used.

5. Long-term evolution and discussion

As shown in Fig. 9 for the double-cluster experiment with the initial PV anomaly centered at $r = 50$ km, after

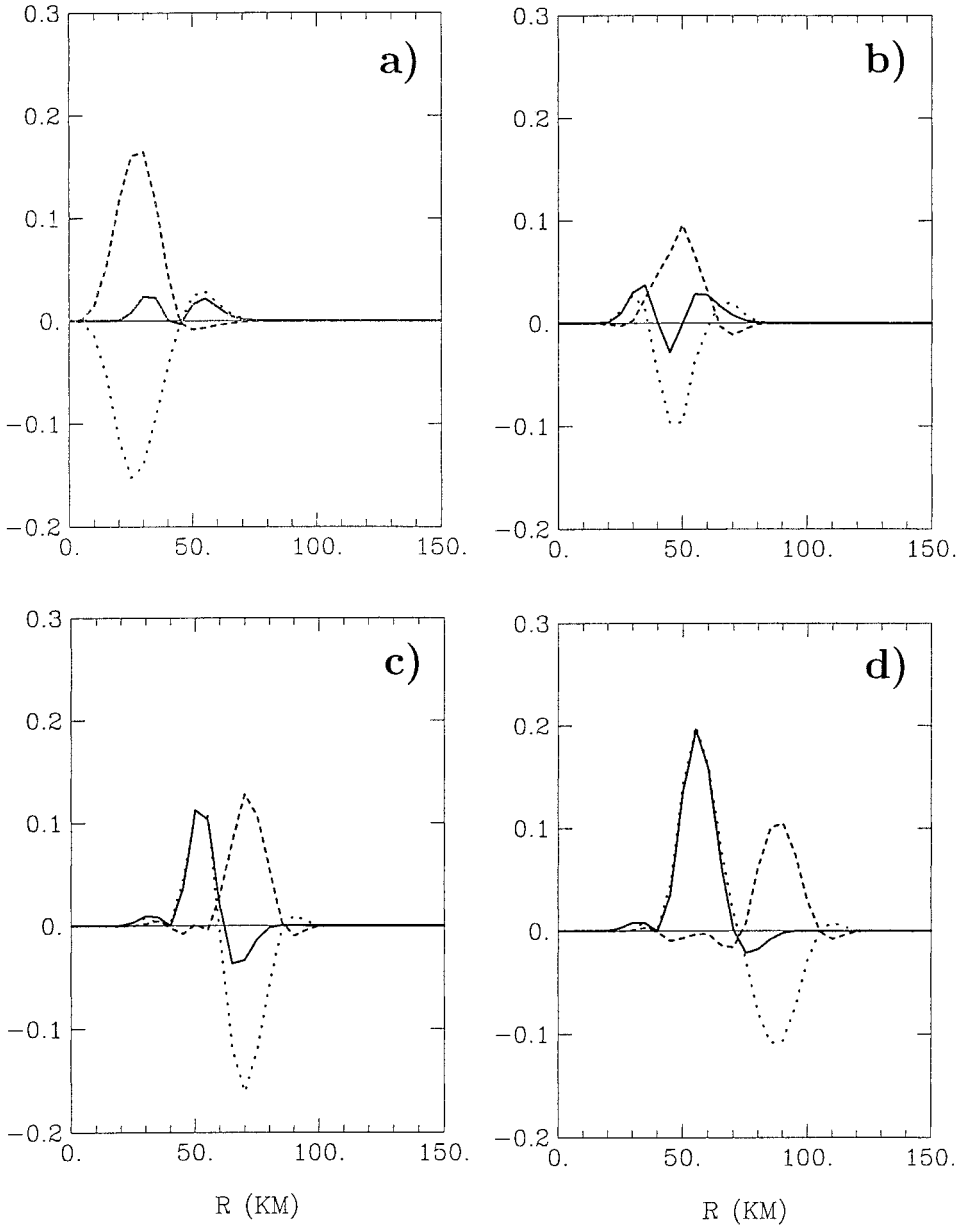

FIG. 10. Horizontal eddy vorticity flux term (solid line), total advective time change terms (dotted line), and their difference (dashed line) [all $\times 10^{-11}$ s^{-3}] after 30 min (time = 24 h, 30 min) for middle layer in double-cluster experiments centered at r = (a) 30 km, (b) 50 km, (c) 70 km, (d) 90 km.

30 min, there is a decrease in vorticity ($\Delta\overline{\zeta}_2 < 0$) at $r \sim 45$ km, the location of maximum $\overline{w}_{BL}$ (Figs. 3b and 13); since $\Delta\overline{w}_{BL}$ is approximately $\propto\Delta\overline{\zeta}_2$ (Ekman-like convergence), the maximum in $\overline{w}_{BL}$ is reduced (Fig. 13). The reduction in the maximum in $\overline{w}_{BL}$ and corresponding convective mass flux by the asymmetry would be expected to lead to a net weakening of the symmetric vortex. Such a weakening does, in fact, occur within ~18 h after the addition of the PV anomaly. Since the benchmark experiment (section 3) and all of the double-cluster experiments (section 4) have the same qualitative response at early times, including the decrease of $\overline{\zeta}_2$ at the location of maximum $\overline{w}_{BL}$, weakening occurs in all of these cases. Figure 14 shows the evolution of the symmetric vortex in the benchmark experiment after 6, 12, and 24 h. By 6 h (time = 30 h; Fig. 14a), the contributions from the horizontal eddy fluxes to the change of the symmetric vortex have become very small, and the symmetric contributions dominate (Fig. 6d). After 12 h, the change in the middle-layer tangential wind (time = 36 h; Fig. 14b) has reversed from earlier times, with a deceleration inside the RMW and a stron-

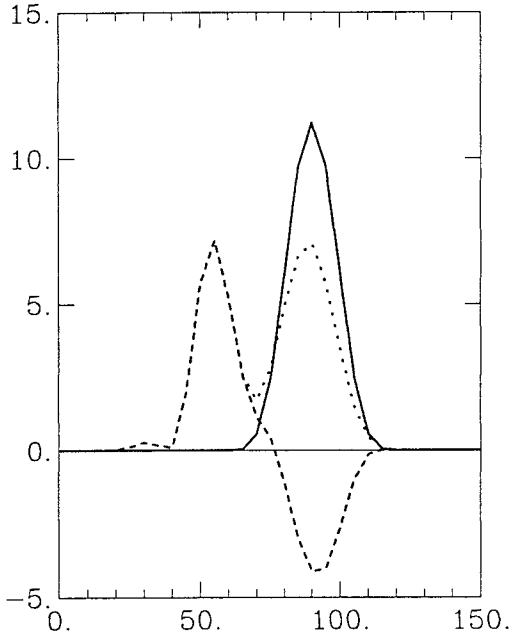

FIG. 11. Initial (solid line), final (dotted line), and change (dashed line) in middle-layer wave activity, $\overline{\zeta_2'^2}$ ($\times 10^{-9}$ s^{-2}), after 30 min (time = 24 h, 30 min) in double-cluster experiment centered at r = 90 km.

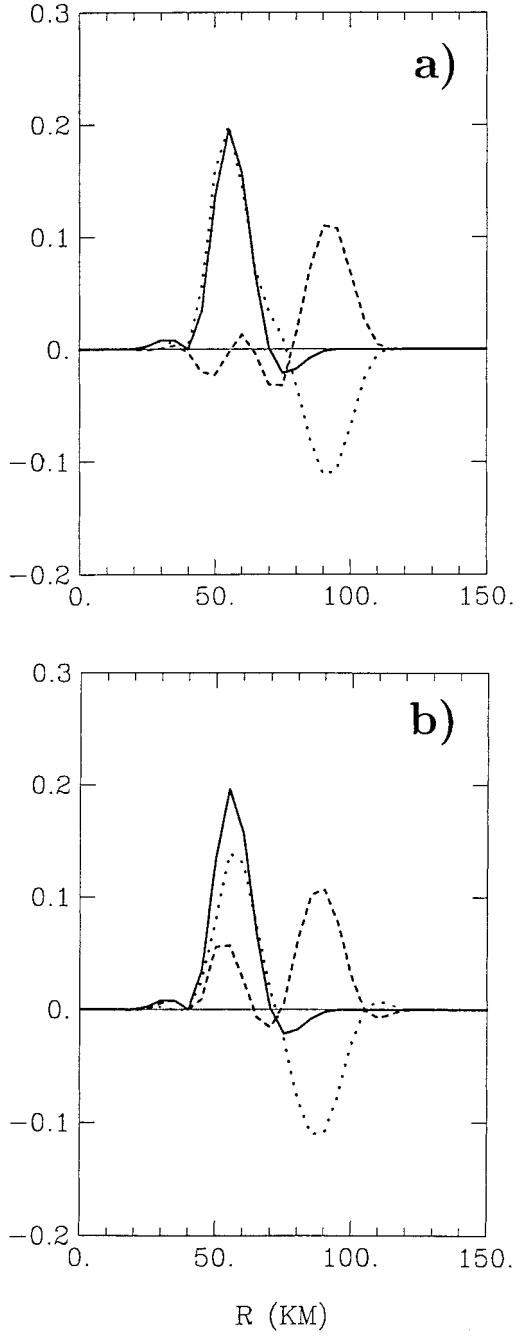

FIG. 12. (a) Horizontal eddy vorticity flux term (solid line), local time change of wave activity (dotted line), and their difference (dashed line) [all $\times 10^{-11}$ s^{-3}] after 30 min (time = 24 h, 30 min) for the middle layer in double-cluster experiment centered at r = 90 km. (b) Same as (a) but for total advective time change terms + divergence terms (dotted line) instead of local time change.

ger acceleration outside. At this time, the vortex has still intensified due to the asymmetry, with $\Delta p_s = -0.07$ mb. After 24 h, however, the deceleration inside the RMW ($\Delta\overline{V}_2 = -1.5$ m s^{-1}) is greater than the acceleration outside (time = 48 h; Fig. 14c), and the vortex has filled, with $\Delta p_s = 1.03$ mb.

The fate of the symmetric vortex is determined in a very short time. Even at early times, the asymmetric PV anomaly in the moist experiments produces changes in the symmetric vortex (sections 3 and 4) that have significant differences from those in dry experiments (section 2) or previous barotropic studies (MK97 and MM99). A diagnosis of the contributions to changes in the symmetric wind tendency due to the asymmetry (section 3) confirm the dominance of horizontal eddy fluxes at the early times. The barotropic eddy kick provided by the asymmetry lasts ~2 h, which is the damping timescale for the disturbance (section 4).

The PV maximum inside the RMW has a prominent role in determining the symmetric response. As demonstrated using a vorticity budget for the disturbance (section 4), the changes in the symmetric wind tendency due to the asymmetry can be most simply explained by a combination of horizontal advection and damping of wave activity. Although divergence also has a nonnegligible contribution, it is effectively balanced by diffusive damping. In conjunction with horizontal advection and damping, the reversal of the radial vorticity gradient associated with the PV maximum constrains the asymmetries to reduce the maximum middle-layer tangential wind as well as the symmetric vorticity near the RMW. The location of the PV maximum controls the response to the extent that moving the PV anomaly radially inward or outward has no qualitative effect on the results. This behavior is unlike that anticipated from

wave activity arguments for the dry experiments (section 2) or previous barotropic studies. As noted at the end of section 4, the interactions between the asymmetries and the symmetric hurricane vortex at early times depend on realistic features of the model hurricane, including the local PV maximum, and not on interactions between the asymmetries and the boundary layer, which possibly depend on the convective parameterization.

The later evolution of the symmetric vortex is more complicated than envisioned in the barotropic studies, where the asymmetries always tended to produce a net intensification of the vortex. Although the symmetric vortex in the present moist experiments intensifies at early times, it weakens within ~18 h. This weakening may depend on the convective parameterization used. The present three-layer model parameterizes the convection in terms of a measure of moist instability and a convective mass flux proportional to boundary layer convergence. Surface enthalpy fluxes destabilize the atmosphere but do not directly drive the convection. The long-term weakening of the vortex in the present experiments is likely due to the reduction in the maximum convective mass flux. An alternate convective parameterization in terms of boundary layer equilibrium (Emanuel 1995) could change the net influence of the asymmetries in the long-term evolution of the tropical cyclone. It should be noted, however, that not only the maximum convective mass flux is reduced in all of the moist experiments but also the maximum middle-layer tangential wind (see Fig. 5 for the benchmark experiment and Fig. 8 for the double-cluster experiments). In a convective parameterization, such as that of Emanuel (1995) or Emanuel (1986), where convective activity is more directly related to surface enthalpy fluxes, such a reduction in maximum wind would be expected to weaken the maximum convective activity as well. The validity of convergence-based convective parameterizations, such as Ooyama's (1969), versus surface flux-based parameterizations, such as Emanuel's (1995), is a subject of current controversy.[5]

An alternate parameterization of the horizontal diffusion with a coefficient other than the divergence-dependent one in the present model could also change the results. Modification of the convective or diffusive parameterization is beyond the scope of the present paper. Nevertheless, the central result developed in sections 3 and 4, which showed that at early times, the asymmetry acts as an eddy kick that intensifies the symmetric vortex

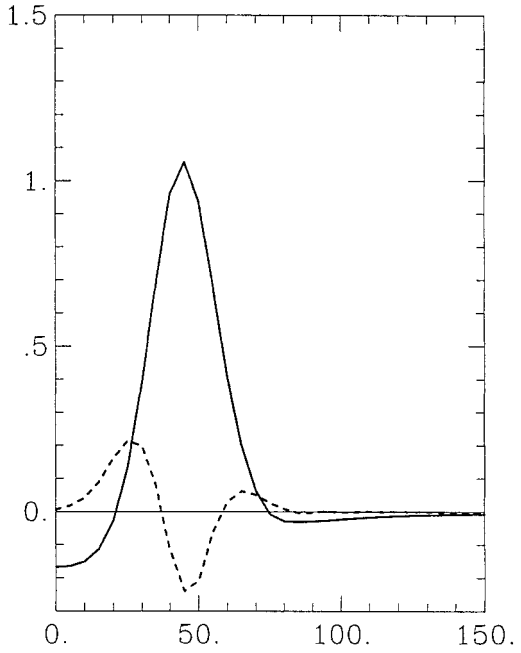

FIG. 13. Vertical velocity at the top of the boundary layer, $\overline{w}_{BL}$ (m s^{-1}; solid line), and change, $\Delta\overline{w}_{BL}$ (10^{-2} m s^{-1}; dashed line), after 30 min (time = 24 h, 30 min) in double-cluster experiments centered at r = 50 km.

in an effectively barotropic process, should be independent of the parameterizations. Although the details of the long-term evolution of the symmetric vortex are more problematic, the reversal of the vorticity gradient associated with the convectively forced PV maximum near the RMW would be expected to play an important role in that development as it does in the present study.

Within the context of the present model, further studies are required to determine the dependence of the results on the amplitude, the radial and tangential scale of the asymmetric PV disturbance, and its vertical structure. The horizontal diffusion coefficient for the symmetric vortex had a magnitude $\sim 2 \times 10^4$ m^2 s^{-1} at the RMW, which is consistent with the effective damping rate $\sim 1.4 \times 10^{-4}$ s^{-1} found in section 4, and a length scale for the disturbance ~ 12 km. Increasing the length scale of the disturbance would decrease the effective damping rate, which could influence the results. The amplitude of the PV anomaly was 20% of the basic state value, a weak disturbance on the vortex; the symmetric response was correspondingly very small. Increasing the amplitude of the disturbance could also influence the results. For small-amplitude disturbances, the symmetric response will be approximately proportional to the square of the disturbance amplitude; doubling the amplitude will approximately quadruple the symmetric response. Also, the present experiments used a single initial PV anomaly ''pulse.'' Multiple-pulsing experiments have been shown to lead to realistic rates of cyclogenesis (ME98) when the PV anomalies are added at intervals ~one half the eddy turnover time for the vortex; a sim-

[5] See Ooyama (1982) for a discussion of conditional instability of the second kind (CISK) and convergence-based schemes in the context of hurricane development, Craig and Gray (1996) for a critical analysis of CISK, and Ooyama (1997) for a response. See also Stevens et al. (1997) for a comment on a criticism of CISK by Emanuel et al. (1994) and their reply (Emanuel et al. 1997), and see Smith (1997b) for a discussion of the theory of CISK and its relation to the surface flux-based parameterizations.

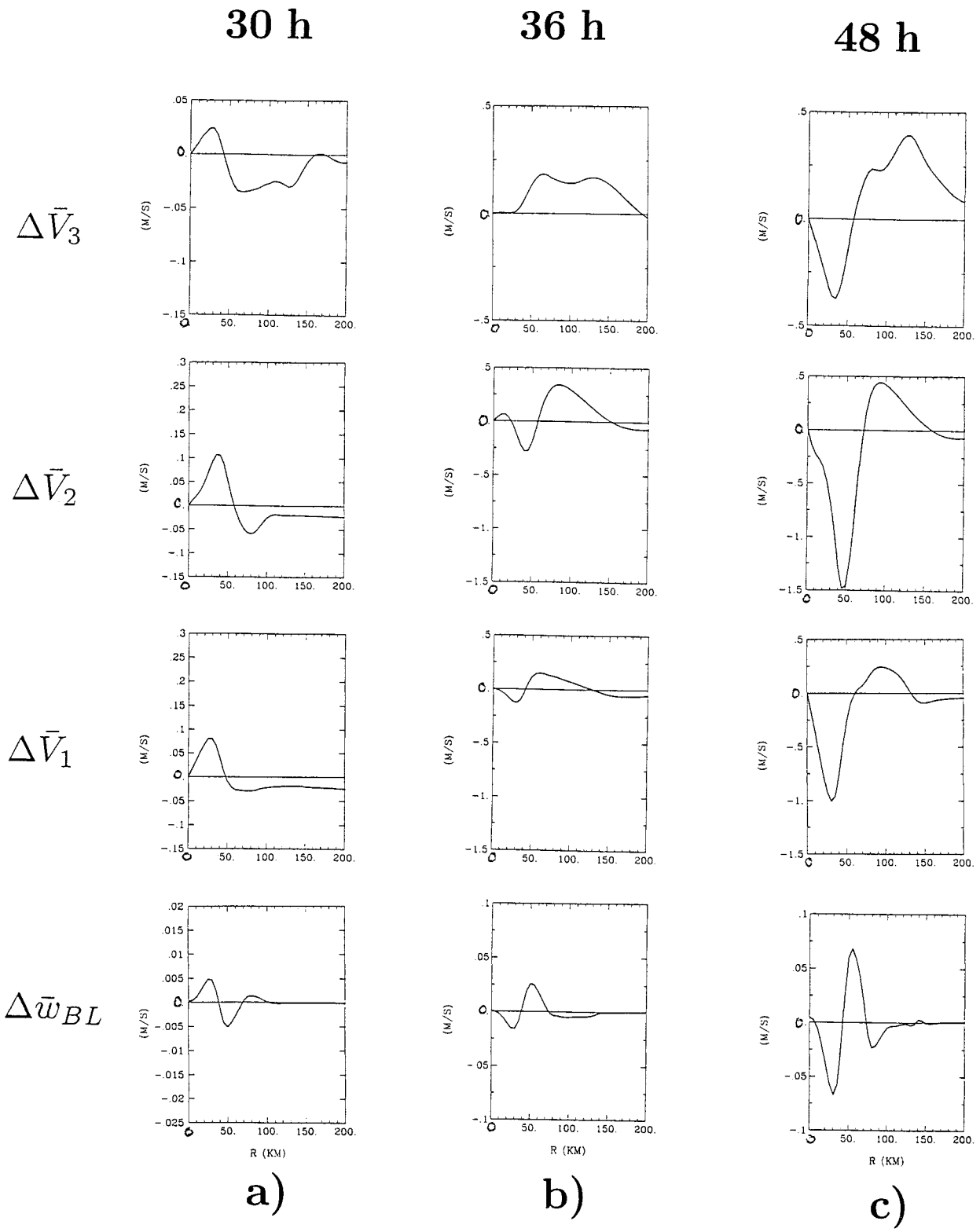

FIG. 14. Same as Fig. 5 after (a) 6 h (time = 30 h), (b) 12 h (time = 36 h), (c) 24 h (time = 48 h). Note different vertical scale in (b) and (c).

ilar result has been recently found for an intensifying tropical stormlike vortex by Möller and Montgomery (2000) using the asymmetric balance formulation of Shapiro and Montgomery (1993). The response to larger-amplitude disturbances and to multiple PV pulses are other areas for further investigation. In order to keep the experimental design as simple as possible, the PV anomaly was confined to the lower two layers of the model (see footnote 3). A convectively forced disturbance, however, will have opposite-signed PV overlying the lower-level anomaly. The role of this upper-level PV in the evolution of the vortex should be investigated as well. Experiments designed to evaluate the effect of each of these quantitities on the short- and long-term evolution of the tropical cyclone vortex are in progress and will be reported on separately in due course.

Acknowledgments. This research was supported in part by the Office of Naval Research Grant N00014-93-1-0456 to Colorado State University and Grant N00014-95-1-0394 to the University of Munich. Much of the research was completed while the author was a Visiting Scientist in the Department of Atmospheric Science, Colorado State University. Discussions with Drs. Dominique Möller and Michael Montgomery during the course of this work were of considerable value.

REFERENCES

Craig, G. C., and S. L. Gray, 1996: CISK or WISHE as the mechanism for tropical cyclone intensification. *J. Atmos. Sci.,* **53,** 3528–3540.

DeMaria, M., and J. D. Pickle, 1988: A simplified system of equations for simulation of tropical cyclones. *J. Atmos. Sci.,* **45,** 1542–1554.

——, S. D. Aberson, K. V. Ooyama, and S J. Lord, 1992: A nested spectral model for hurricane track forecasting. *Mon. Wea. Rev.,* **120,** 1628–1643.

Emanuel, K. A., 1986: An air–sea interaction theory for tropical cyclones. Part I: Steady state maintenance. *J. Atmos. Sci.,* **43,** 585–604.

——, 1995: The behavior of a simple hurricane model using a convective scheme based on subcloud-layer entropy equilibrium. *J. Atmos. Sci.,* **52,** 3960–3968.

——, J. D. Neelin, and C. S. Bretherton, 1994: On large-scale circulations in convecting atmospheres. *Quart. J. Roy. Meteor. Soc.,* **120,** 1111–1143.

——, ——, and ——, 1997: Reply to 'Comments' by Stevens, Randall, Lin and Montgomery. *Quart. J. Roy. Meteor. Soc.,* **123,** 1779–1782.

Gent, P., and J. McWilliams, 1986: The instability of barotropic circular vortices. *Geophys. Astrophys. Fluid Dyn.,* **35,** 209–233.

Guinn, T. A., and W. H. Schubert, 1993: Hurricane spiral bands. *J. Atmos. Sci.,* **50,** 3380–3403.

Held, I. M., and B. J. Hoskins, 1985: Large-scale eddies and the general circulation of the troposphere. *Advances in Geophysics,* Vol. 28A, Academic Press, 3–31.

Jorgensen, D. P., 1984: Mesoscale and convective-scale characteristics of mature hurricanes. Part II: Inner core structure of Hurricane Allen (1980). *J. Atmos. Sci.,* **41,** 1287–1311.

Molinari, J., and D. Vollaro, 1989: External influences on hurricane intensity. Part I: Outflow layer eddy angular momentum fluxes. *J. Atmos. Sci.,* **46,** 1093–1105.

——, S. Skubis, and D. Vollaro, 1995: External influences on hurricane intensity. Part III: Potential vorticity structure. *J. Atmos. Sci.,* **52,** 3593–3606.

Möller, J. D., and M. T. Montgomery, 1999: Vortex Rossby waves and hurricane intensification in a barotropic model. *J. Atmos. Sci.,* **56,** 1674–1687.

———, and ———, 2000: Tropical cyclone evolution via potential vorticity anomolies in a three-dimensional balance model. *J. Atmos. Sci.,* **57,** 3366–3387.

Montgomery, M. T., and L. J. Shapiro, 1995: Generalized Charney–Stern and Fjortoft theorems for rapidly rotating vortices. *J. Atmos. Sci.,* **52,** 1829–1833.

——, and R. J. Kallenbach, 1997: A theory for vortex Rossby waves and its application to spiral bands and intensity changes in hurricanes. *Quart. J. Roy. Meteor. Soc.,* **123,** 435–465.

——, and J. Enagonio, 1998: Tropical cyclogenesis via convectively forced vortex Rossby waves in a three-dimensional quasigeostrophic model. *J. Atmos. Sci.,* **55,** 3176–3207.

Ooyama, K. V., 1969: Numerical simulation of the life cycle of tropical cyclones. *J. Atmos. Sci.,* **26,** 3–40.

——, 1982: Conceptual evolution of the theory and modelling of the tropical cyclone. *J. Meteor. Soc. Japan,* **60,** 369–380.

——, 1984: A model for hurricane prediction. Postprints, *15th Conf. on Hurricanes and Tropical Meteorology,* Boston, MA, Amer. Meteor. Soc., 344–349.

——, 1997: Footnotes to ''Conceptual evolution.'' Preprints, *22d Conf. on Hurricanes and Tropical Meteorology,* Fort Collins, CO, Amer. Meteor. Soc., 13–18.

Pfeffer, R. L., 1958: Concerning the mechanism of hurricanes. *J. Meteor.,* **15,** 113–120.

——, and M. Challa, 1981: A numerical study of the role of eddy fluxes of momentum in the development of Atlantic hurricanes. *J. Atmos. Sci.,* **38,** 2393–2398.

Raymond, D. J., 1995: Regulation of moist convection over the west Pacific warm pool. *J. Atmos. Sci.,* **52,** 3945–3959.

Shapiro, L. J., 1992: Hurricane vortex motion and evolution in a three-layer model. *J. Atmos. Sci.,* **49,** 140–153.

——, 1998: Convective asymmetries and tropical cyclone evolution. Preprints, *Symp. on Tropical Cyclone Intensity Change,* Phoenix, AZ, Amer. Meteor. Soc., 80–81.

——, 1999: Convective asymmetries and tropical cyclone evolution in a three-layer model. Preprints, *23d Conf. on Hurricanes and Tropical Meteorology,* Dallas, TX, Amer. Meteor. Soc., 682–683.

——, and M. T. Montgomery, 1993: A three-dimensional balance theory for rapidly rotating vortices. *J. Atmos. Sci.,* **50,** 3322–3335.

——, and J. L. Franklin, 1995: Potential vorticity in Hurricane Gloria. *Mon. Wea. Rev.,* **123,** 1465–1475.

Smith, R. K., Ed., 1997a: The physics and parameterization of moist atmospheric convection. *Proceedings of the NATO Advanced Study Institute,* Kluwer Academic, 498 pp.

——, 1997b: On the theory of CISK. *Quart. J. Roy. Meteor. Soc.,* **123,** 407–418.

Stevens, B., D. A. Randall, X. Lin, and M. T. Montgomery, 1997: Comments on 'On large-scale circulations in convecting atmospheres' by Emanuel, Neelin and Bretherton. *Quart. J. Roy. Meteor. Soc.,* **123,** 1771–1778.

Willoughby, H. E., 1995: Mature structure and evolution. Global Perspectives on tropical cyclones. Tropical Cyclone Programme Rep. TCP-38, WMO/TD-693, Geneva, Switzerland, 289 pp.

——, H. E., J. A. Clos, and M. G. Shoreibah, 1982: Concentric eye walls, secondary wind maxima, and the evolution of the hurricane vortex. *J. Atmos. Sci.,* **39,** 395–411.

——, F. D. Marks Jr., and R. J. Feinberg, 1984: Stationary and moving convective bands in hurricanes. *J. Atmos. Sci.,* **41,** 3189–3211.